

Hafnium Resonance Parameter Analysis Using Neutron Capture and Transmission Experiments

M. J. Trbovich,*† D. P. Barry,† R. E. Slovacek, Y. Danon, R. C. Block,
N. C. Francis, and M. Lubert

*Rensselaer Polytechnic Institute, Mechanical, Aerospace and Nuclear Engineering Department
Troy, New York 12180-3590*

and

J. A. Burke, N. J. Drindak, G. Leinweber, and R. Ballad

Knolls Atomic Power Laboratory, P.O. Box 1072, Schenectady, New York 12301-1072

Received July 23, 2007

Accepted June 27, 2008

Abstract—*The focus of this work is to determine the resonance parameters for stable hafnium isotopes in the 0.005- to 200-eV region, with special emphasis on the overlapping ^{176}Hf and ^{178}Hf resonances near 8 eV. Accurate hafnium cross sections and resonance parameters are needed in order to quantify the effects of hafnium found in zirconium, a metal commonly used in reactors. The accuracy of the cross sections and the corresponding resonance parameters used in current nuclear analysis tools are rapidly becoming the limiting factor in reducing the overall uncertainty on reactor physics calculations.*

Experiments measuring neutron capture and transmission are routinely performed at the Rensselaer Polytechnic Institute LINAC using the time-of-flight technique. Lithium-6 glass scintillation detectors were used for transmission experiments at flight path lengths of 15 and 25 m, respectively. Capture experiments were performed using a 16-section NaI multiplicity detector at a flight path length of 25 m. These experiments utilized several thicknesses of metallic and isotope-enriched liquid Hf samples. The liquid Hf samples were designed to provide information on the ^{176}Hf and ^{178}Hf contributions to the 8-eV doublet without saturation.

Data analyses were performed using the R-matrix Bayesian code SAMMY. A combined capture and transmission data analysis yielded resonance parameters for all hafnium isotopes from 0.005 to 200 eV. Additionally, resonance integrals were calculated, along with errors for each hafnium isotope, using the NJOY and INTER codes. The isotopic resonance integrals calculated were significantly different from previous values. The ^{176}Hf resonance integral, based on this work, is $\sim 73\%$ higher than the ENDF/B-VI value. This is due primarily to the changes to resonance parameters in the 8-eV resonance; the neutron width presented in this work is more than twice that of the previous value. The calculated elemental hafnium resonance integral, however, changed very little.

I. INTRODUCTION

The majority of measurements and analyses of hafnium cross sections in the region below 200 eV were performed prior to 1965. There were a few measurements by Liou et al.¹ and Moxon et al.² made in the mid-1970s. However, most of the ENDF/B-VI reso-

nance parameters for hafnium in this region are based on much older experiments. These older experiments provided lower-resolution data and, because of the tight level spacing of hafnium, led to many missed resonances. An example of this is best shown in the case of the resonance pair near 8 eV.

A very strong resonance (~ 25 kb) near 8 eV was attributed solely to ^{178}Hf up until 1974, when measurements by Moxon et al.² showed the existence of a ^{176}Hf resonance at nearly the same energy. Although this new resonance made no significant impact on the total neutron

*E-mail: trbovmj@kapl.gov

†Current address: Knolls Atomic Power Laboratory, P.O. Box 1072, Schenectady, New York 12301-1072

cross section for natural hafnium, it did affect the way the hafnium interactions would change with exposure to a neutron flux. This is one example of the importance of accurate resonance parameters for analysis of nuclear systems.

The work described in this paper was completed at the Rensselaer Polytechnic Institute (RPI) LINAC facility and is described more thoroughly in the doctoral thesis³ found on file at the RPI library.

II. EXPERIMENTAL SETUP

Transmission experiments at the RPI LINAC are performed in two primary configurations, referred to as “thermal” and “epithermal.” Thermal transmission experiments are optimized for low energies (0.001 to 20 eV) and utilize an ~ 15 -m flight path arrangement. This short flight path provides for a higher intensity of neutrons. The detector used at the ~ 15 -m station is a 5.08-cm (2-in.)-diam and 3-mm-thick ^6Li loaded glass scintillator that is optically coupled to a photomultiplier tube (PMT). A more detailed description of the complete experimental setup at the RPI LINAC can be found in Ref. 4. The samples for the thermal transmission experiments are mounted on a sample changer that is located ~ 14 m from the neutron production target. The neutron production target used for thermal transmission experiments is the enhanced thermal target.⁵ This target is designed to provide the low-energy neutrons needed for these experiments.

Epithermal transmission experiments are done with a detector ~ 25 m away from the neutron production target. This detector is a 12.7-cm (5-in.)-diam and 1.27-cm (0.5-in.)-thick ^6Li loaded glass scintillator that is optically coupled to a PMT. A rotary sample changer is located ~ 14 m away from the neutron production target.

The target used to produce neutrons for the epithermal transmission measurements is known as the bounce target⁶ and more recently as the bare bounce target.⁷ These targets are designed for neutron measurements from a few electron volts up to ~ 1 keV.

Capture experiments at the RPI LINAC are performed using a 16-segment NaI(Tl) multiplicity-type detector.⁸ This detector is located ~ 25 m from the neutron production target. Samples are inserted into the center of the detector and held in place by hollow aluminum tubes. Eight samples can be mounted on a wheel that translates and rotates in order to change samples. The detector is inside a 15.24-cm (6-in.)-thick lead shield with through-holes for the neutron beam and sample insertion and extraction.

III. HAFNIUM SAMPLES

The majority of resonances in hafnium below 200 eV were measured using various thicknesses of metallic natural hafnium. The metal samples were all of natural isotopic abundance and were in the form of disks with ~ 5.08 -cm (2-in.) diameters. The sample thicknesses of the metallic hafnium used are given in Table I along with the experiments they were used in. This variation in sample thickness enabled the analysis of widely ranging cross sections for the many resonances in hafnium below 200 eV.

The metallic samples did not allow for accurate analysis of the pair of resonances near 8 eV. The total cross section due to the 8-eV resonance pair is predicted to be as high as 30 000 b. This extremely large cross section at 8 eV ensures that this resonance is saturated in all but the two thinnest metallic samples.

Liquid samples were used in experiments specifically designed for analysis of the 8-eV pair of overlapping ^{176}Hf and ^{178}Hf resonances. The large cross section of this resonance pair (~ 30 000 b) required an extremely

TABLE I
Metallic Hafnium Sample Specifications*

Thickness			Experiment(s) Used In			
Nominal (cm)	Nominal (mil) ^a	N (atom/b)	Thermal Transmission	Thermal Capture	Epithermal Transmission	Epithermal Capture
0.00127	0.5	4.621×10^{-5}				X
0.00254	1	9.984×10^{-5}	X			
0.00508	2	2.369×10^{-4}	X	X		X
0.01016	4	4.537×10^{-4}	X	X		
0.0254	10	1.139×10^{-3}	X	X	X	X
0.0508	20	2.303×10^{-3}	X		X	
0.127	50	5.755×10^{-3}	X		X	X
0.254	100	1.154×10^{-2}			X	

^a1 mil = 0.001 in.

TABLE II
Isotopic Abundance of Enriched Hafnium Samples

	¹⁷⁴ Hf (at.%)	¹⁷⁶ Hf (at.%)	¹⁷⁷ Hf (at.%)	¹⁷⁸ Hf (at.%)	¹⁷⁹ Hf (at.%)	¹⁸⁰ Hf (at.%)	Total Mass (u)
Enriched ¹⁷⁶ Hf	0.08	56.17	26.96	10.60	2.49	3.71	176.72
Enriched ¹⁷⁸ Hf	1.50	1.78	4.20	83.37	5.58	3.56	177.97
Nat Hf	0.162 ^a	5.206 ^a	18.606 ^a	27.297 ^a	13.629 ^a	35.100 ^a	178.49

^aThese isotopic abundance values are from the *Chart of the Nuclides*.

thin sample for adequate experimental capture and transmission data. Metal foils could not feasibly be fabricated thin enough with adequate quality for these experiments. The liquid samples provide a more uniform thickness than metal, and the thickness can be controlled by the hafnium concentration in the solution.

The liquid samples were created using both natural hafnium oxide and hafnium oxides enriched in ¹⁷⁸Hf and ¹⁷⁶Hf. The isotopic content of the enriched oxides was measured using a mass spectrometer. Table II shows the results of the mass spectrometer analysis of the enriched hafnium samples in terms of isotopic percentages.

Dissolving the hafnium into a liquid solution was thought to be a superior alternative to solid oxide samples. The solution provides a uniform distribution of hafnium as long as the solution is not near its saturation point. The solvent also has to have a low and constant cross section. It was determined that hafnium could be dissolved into deuterated nitric acid (DNO₃). The DNO₃ provided a low, flat cross section in the energy range of interest for these experiments.

Liquid sample hafnium concentrations were based on hafnium densities that would produce transmission values sufficiently above background and below saturation levels to allow for accurate measurements. The first set of liquid samples was called "generation I." Table III shows the properties of this generation I set of liquid

samples, indexed by a unique serial number on each cell. The generation I samples were contained in cells made from two ~ 5.08-cm (2-in.)-diam, 0.159-cm (0.0625-in.)-thick quartz flats with a polyvinyl chloride (PVC) spacer ring glued between them with acid-resistant epoxy.

The concentration for each generation I liquid sample is shown in Table III. The concentration of each solution was measured by inductively coupled plasma emission spectroscopy.

After the experiments with the generation I liquid cells, two of the cells were found to have leaks. The leaks were not significant enough to affect the experimental results; however, this prompted a new cell design for the next set of experiments. The new cell design replaced the PVC spacer ring with a quartz ring that was fused in place. This design eliminated the glue joint in the previous generation, which seemed to be the source of leaks. The new cells were referred to as "generation II" cells and were of the same nominal dimensions as the generation I cells. The properties of the generation II liquid samples are given in Table IV.

IV. DATA ANALYSIS

The first hafnium data set analyzed was the epithermal metallic transmission data. The ENDF/B-VI

TABLE III
Generation I Liquid Samples

Cell Number	Type of Hf Dissolved	Nominal Liquid Thickness (in.)	Measured Hf Concentration (mg/cm ³)	Hf Number Density (atom/b)
Hf-1-1	Enriched ¹⁷⁶ Hf	0.09375	44.70 ± 0.408	3.888 × 10 ⁻⁵
Hf-1-2	D ₂ O + DNO ₃ blank	0.09375	—	—
Hf-1-4	Enriched ¹⁷⁸ Hf	0.09375	24.34 ± 0.062	2.017 × 10 ⁻⁵
Hf-1-5	Enriched ¹⁷⁸ Hf	0.09375	12.14 ± 0.072	1.048 × 10 ⁻⁵
Hf-1-6	Enriched ¹⁷⁸ Hf	0.09375	3.07 ± 0.021	2.467 × 10 ⁻⁶
Hf-1-7	Natural	0.09375	35.50 ± 0.146	2.923 × 10 ⁻⁵

TABLE IV
Generation II Liquid Samples

Cell Number	Type of Hf Dissolved	Nominal Liquid Thickness (in.)	Measured Hf Concentration (mg/cm ³)	Hf Number Density (atom/b)
Hf-2-2	D ₂ O + DNO ₃ blank	0.09375	—	—
Hf-2-3	Enriched ¹⁷⁶ Hf	0.09375	26.6 ± 0.5	2.183 × 10 ⁻⁵
Hf-2-4	Enriched ¹⁷⁶ Hf	0.09375	9.07 ± 0.18	6.949 × 10 ⁻⁶
Hf-2-5	Enriched ¹⁷⁶ Hf	0.09375	4.15 ± 0.08	3.639 × 10 ⁻⁶
Hf-2-6	Enriched ¹⁷⁸ Hf	0.09375	1.63 ± 0.08	1.367 × 10 ⁻⁶
Hf-2-7	Enriched ¹⁷⁸ Hf	0.09375	0.89 ± 0.045	6.868 × 10 ⁻⁷

resonance parameters were used as starting parameters for the SAMMY fit⁹ to the data. A combined fit was performed on the 0.0254-cm (10-mil), 0.0508-cm (20-mil), 0.127-cm (50-mil), and 0.254-cm (100-mil) metallic sample data. This was done by fitting each data set sequentially and using the SAMMY parameter file along with the SAMMY covariance matrix file created by the previous fit as input to the next. After a fit to the transmission data sets with a minimum χ_r^2 (reduced chi-squared³) was achieved, epithermal metallic capture data sets were added to the combined analysis. The 0.00127-cm (0.5-mil), 0.00508-cm (2-mil), 0.0254-cm (10-mil), and 0.127-cm (50-mil) sample capture data were added to the fitting sequence of epithermal transmission data sets to form a combined fit. This combined fit sequence was run until a minimum χ_r^2 was achieved.

Not all of the resonance parameters were allowed to vary during the SAMMY fit. If a radiation width parameter Γ_γ did not affect the overall fit and was allowed to vary, it was found that the value of this Γ_γ parameter could “run away.” This meant the radiation width value would continuously increase or decrease with each run of SAMMY without converging. In such cases, the Γ_γ parameter was fixed to an average value of the radiation widths for that particular isotope. This average value of Γ_γ was found by averaging the “sensitive” Γ_γ values that were fit by SAMMY within each isotope. Barry¹⁰ developed the criteria used to determine which Γ_γ values should be varied. The method was based on the ratio of the radiation width to the neutron width Γ_γ/Γ_n and was used to give a sensitivity factor for Γ_γ . The cases where the ratio was ≤ 5 gave good indication the fit would be sensitive to Γ_γ . This solved the problem for most of the insensitive Γ_γ values that were running away. However, there were still a few Γ_γ values that were deemed sensitive based on the Barry¹⁰ criteria that did not converge. These cases were found in resonances that overlapped a neighboring resonance (or several resonances). In some of these cases one Γ_γ would constantly change while being compen-

sated for by a nearby resonance’s Γ_γ changing in the opposite direction. Through trial-and-error SAMMY runs, these parameters were also fixed to an average value of Γ_γ based on the Γ_γ values that did converge for that particular isotope.

The average Γ_γ for each isotope was calculated from a weighted average of the converged Γ_γ values for that isotope. All of the insensitive Γ_γ values were fixed to this average value for that isotope, and the fit was repeated in an iterative fashion. This iteration continued until the calculated average Γ_γ for each isotope agreed with the previous iteration’s average Γ_γ .

When no further improvements in the fit were apparent and the resonance parameters remained unchanged relative to the previous iteration, the parameters were deemed final. SAMMY was then used to calculate transmission and capture curves based on these final resonance parameters to compare with the experimental data from each sample.

After the resonance parameters were determined for the epithermal region (10 to 200 eV), the thermal data were then analyzed using SAMMY. The thermal transmission data set was analyzed first, and the capture data were added to the analysis once reasonable transmission fits were achieved. The combined analysis of the 0.00254-cm (1-mil), 0.00508-cm (2-mil), 0.01016-cm (4-mil), 0.0254-cm (10-mil), 0.0508-cm (20-mil), and 0.127-cm (50-mil) thermal transmission samples and the 0.00508-cm (2-mil), 0.01016-cm (4-mil), and 0.0254-cm (10-mil) thermal capture samples were run in SAMMY until a minimum χ_r^2 was achieved and there were no significant changes in parameters between runs.

The insensitivity of the low-energy resonances to the energy resolution and the Doppler broadening effect allows accurate simultaneous determination of all resonance parameters below 10 eV.

The resonance doublet at 8 eV was not analyzed using the metallic sample data, as it was saturated or close to saturation and provided little information. The thinner isotope-enriched liquid sample data were used to determine the parameters for these resonances.

A sample of the transmission and capture fitted curves and data is shown in Fig. 1. The 0.0254-cm (10-mil) metallic capture sample shown in Fig. 1 shows the effect of a strong resonance with approximately equal scattering and capture probabilities in a relatively thick sample. This effect produces a depression at the resonance energy that is due to the high scattering cross section at the resonance energy, which scatters a large portion of neutrons away from the sample before penetrating the surface. Neutrons that have energies slightly above or below the resonance energy have a much higher probability of penetrating the sample but will most likely interact inside the sample. The neutrons that scatter once inside the sample will most likely be captured before leaving the sample, creating increased counts in the wings of the resonance. Table V contains the final resonance parameters determined from this analysis, which all of these fits are based on.

The resonance parameters for the ^{176}Hf and ^{178}Hf resonances near 8 eV were determined from the isotope-enriched liquid sample data. Two generations of these samples were run in both capture and transmission experiments, as described previously. The transmission experiment data using the generation I and II liquid samples were analyzed first using SAMMY. Once the transmission data

were fitted, the capture data were added to the analysis. The combined transmission and capture analysis showed significant differences between the data sets. The yield values from the capture data did not agree with the transmission data over the energy range being analyzed. Because of this, SAMMY was initially unable to determine a set of parameters that fit all of these data sets.

In order to determine if there was a problem with the flux normalization of the capture data or if there was a difference in detection efficiency between isotopes, the 8-eV resonance parameters fitted to the transmission data were used to calculate the expected yield for the capture experiments using SAMMY. The energy region being analyzed was increased to include surrounding ^{177}Hf resonances. The parameters for these resonances had been determined from the previously described analyses using natural metallic samples. The yield curve, calculated from the transmission data, was then applied to the capture data for comparison; Fig. 2 shows this comparison for a ^{176}Hf -enriched liquid sample. Figure 2 shows that the region over the 8-eV doublet is the only area of significant disagreement. The surrounding ^{177}Hf resonances in Fig. 2 show good agreement between the yield data and the calculated yield from the transmission fitted resonance parameters. The lower yield data over the 8-eV

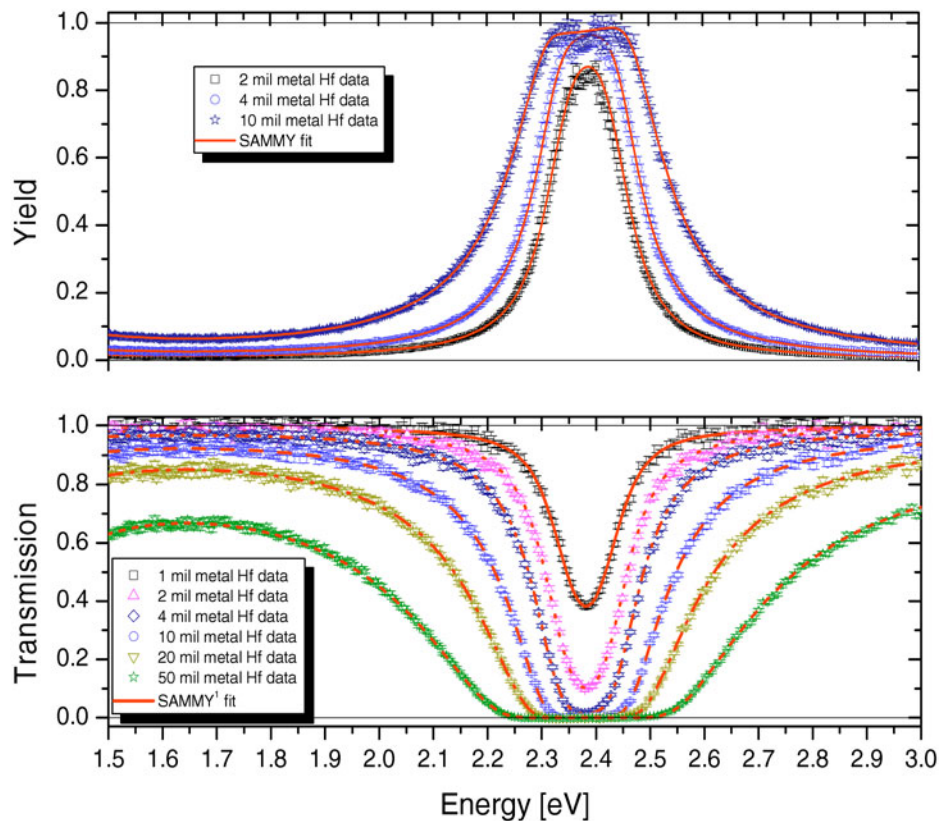


Fig. 1. Thermal metallic hafnium transmission and capture data with SAMMY calculated transmission from fitted resonance parameters.

TABLE V
Fitted RPI Resonance Parameters Compared to ENDF/B-VI and Those Measured by Moxon et al.^{2*}

Energy (eV)			Γ_γ (meV)			Γ_n (meV)			Isotope and Spin
RPI	ENDF/B-VI	Moxon et al. ²	RPI	ENDF/B-VI	Moxon et al. ²	RPI	ENDF/B-VI	Moxon et al. ²	
¹⁷⁴ Hf									
-0.990	-0.99		60.3	60.3		2.29	2.29		174 I = 0 J = $\frac{1}{2}$
4.06 (0.04)	4.25	—	52 (5) [0.002]	60	—	0.015 (0.001) [0.0000]	0.017	—	174 I = 0 J = $\frac{1}{2}$
13.373 (0.004)	13.38	13.38 0.003	65 {29}	60	—	5.7 (0.2) [0.05]	4.8	3.657 0.75	174 I = 0 J = $\frac{1}{2}$
29.985 (0.003)	30	—	65 {29}	60	—	36.3 (0.8) [0.1]	40	—	174 I = 0 J = $\frac{1}{2}$
70.66 (0.02)	70.5	—	65 {29}	60	—	12 ^a	12	—	174 I = 0 J = $\frac{1}{2}$
77.85 (0.01)	77.9	—	51 (4) [2]	60	—	65 ^a	65	—	174 I = 0 J = $\frac{1}{2}$
106.95 (0.02)	107.1	—	65 {29}	60	—	122 ^a	122	—	174 I = 0 J = $\frac{1}{2}$
124.36 (0.03)	124.6	—	65. {29}	60	—	50 ^a	50	—	174 I = 0 J = $\frac{1}{2}$
147.63 (0.04)	147.6	—	102 (10) [9]	60	—	120 ^a	120	—	174 I = 0 J = $\frac{1}{2}$
153.40 (0.04)	153.5	—	65 {29}	60	—	85 ^a	85	—	174 I = 0 J = $\frac{1}{2}$
¹⁷⁶ Hf									
-80.0	-80.0	—	60	60	—	380	380	—	176 I = 0 J = $\frac{1}{2}$
-20.0	-20.0	—	60	60	—	27	27	—	176 I = 0 J = $\frac{1}{2}$
7.8891 (0.0003)	7.886	7.8858 0.01	61.8 (0.6) [0.05]	57	57 [12]	10.15 (0.04) [0.009]	4.71	4.71 5.5	176 I = 0 J = $\frac{1}{2}$
48.2540 (0.0009)	48.3	—	49 (0.4) [1]	51	—	107 (0.5) [2]	125	—	176 I = 0 J = $\frac{1}{2}$
53.282 (0.004)	53.3	—	55 {9}	51	—	1.69 (0.03) [0.009]	1.9	—	176 I = 0 J = $\frac{1}{2}$
67.218 (0.002)	67.1	—	55 {9}	51	—	26.0 (0.6) [0.0000]	15	—	176 I = 0 J = $\frac{1}{2}$

(Continued)

TABLE V (Continued)

Energy (eV)			Γ_γ (meV)			Γ_n (meV)			Isotope and Spin
RPI	ENDF/B-VI	Moxon et al. ²	RPI	ENDF/B-VI	Moxon et al. ²	RPI	ENDF/B-VI	Moxon et al. ²	
¹⁷⁶ Hf (Continued)									
124.079 (0.008)	123.9	—	55 {9}	51	—	32 (1) [2]	42	—	176 I = 0 J = $\frac{1}{2}$
177.15 (0.01)	177.1	—	55 {9}	51	—	86 (3) [4]	47	—	176 I = 0 J = $\frac{1}{2}$
¹⁷⁷ Hf									
1.1001 (0.0001)	1.098	1.0964 0.0015	65.23 (0.08) [0.009]	66.2	65.64 2.86	2.225 (0.002) [0.002]	2.171	2.232 0.013	177 I = $\frac{7}{2}$ J = 3
2.3868 (0.0001)	2.388	2.3837 0.0002	60.7 (0.2) [0.009]	60.8	61.74 0.74	8.04 (0.02) [0.006]	8	8.068 0.068	177 I = $\frac{7}{2}$ J = 4
5.9002 (0.0002)	5.89	5.8937 0.0009	62 (0.5) [2]	54.8	65.47 3.34	5.32 (0.02) [0.05]	6.743	5.348 0.127	177 I = $\frac{7}{2}$ J = 3
6.5780 (0.0002)	6.6	6.5691 0.0014	55.6 (0.3) [0.8]	65	64.96 1.76	8.21 (0.03) [0.06]	8.089	8.049 0.048	177 I = $\frac{7}{2}$ J = 4
8.8766 (0.0002)	8.88	8.8388 0.0008	57.3 (0.4) [0.3]	65	64.97 1.73	5.89 (0.02) [0.03]	6.044	5.705 0.088	177 I = $\frac{7}{2}$ J = 4
10.9607 (0.0007)	10.95	10.941 0.009	57 {13}	65	75.52 9.42	0.490 (0.003) [0.002]	0.56	0.497 0.013	177 I = $\frac{7}{2}$ J = 3
13.6810 (0.0008)	13.67	13.687 0.002	57 {13}	65	64.82 6.56	0.603 (0.004) [0.002]	0.702	0.543 0.031	177 I = $\frac{7}{2}$ J = 4
13.9696 (0.0003)	13.96	13.971 0.003	57 {13}	83.7	74.56 4.79	2.71 (0.009) [0.01]	3.314	3.064 0.073	177 I = $\frac{7}{2}$ J = 3
21.9844 (0.0007)	21.97	22.0052 0.0014	57 {13}	65	67.34 5.24	1.7633 (0.009) [0.009]	1.902	1.565 0.041	177 I = $\frac{7}{2}$ J = 4
22.298 (0.002)	22.26	22.3117 0.0061	57 {13}	65	102.6 12.2	0.840 (0.009) [0.002]	0.857	0.759 0.047	177 I = $\frac{7}{2}$ J = 3
23.426 (0.002)	23.44	23.5205 0.008	57 {13}	65	84.6 10.0	1.32 (0.02) [0.03]	1.458	1.59 0.64	177 I = $\frac{7}{2}$ J = 4
25.641 (0.002)	25.64	25.665 0.001	57 {13}	65	—	0.545 (0.008) [0.002]	0.502857	0.473 0.0037	177 I = $\frac{7}{2}$ J = 3
27.0364 (0.0008)	27.01	27.063 0.01	57 {13}	65	88.1 11.0	2.84 (0.02) [0.02]	3.085714	2.78 0.16	177 I = $\frac{7}{2}$ J = 3
31.608 (0.005)	31.58	—	57 {13}	65	—	0.36 (0.01) [0.009]	0.343	—	177 I = $\frac{7}{2}$ J = 3
32.841 (0.001)	32.82	—	57 {13}	65	—	1.30 (0.01) [0.005]	1.404	—	177 I = $\frac{7}{2}$ J = 4

(Continued)

TABLE V (Continued)

Energy (eV)			Γ_γ (meV)			Γ_n (meV)			Isotope and Spin
RPI	ENDF/B-VI	Moxon et al. ²	RPI	ENDF/B-VI	Moxon et al. ²	RPI	ENDF/B-VI	Moxon et al. ²	
¹⁷⁷ Hf (Continued)									
36.095 (0.001)	36.08	—	57 {13}	65	—	3.53 (0.03) [0.03]	3.531	—	¹⁷⁷ $I = \frac{7}{2}$ $J = 3$
36.9805 (0.0008)	36.95	—	57 {13}	56	—	8.92 (0.05) [0.06]	9.689	—	¹⁷⁷ $I = \frac{7}{2}$ $J = 4$
43.082 (0.001)	43.05	—	57 {13}	65	—	5.13 (0.03) [0.03]	5.173333	—	¹⁷⁷ $I = \frac{7}{2}$ $J = 4$
45.165 (0.001)	45.11	—	57 {13}	65	—	3.37 (0.02) [0.02]	3.377778	—	¹⁷⁷ $I = \frac{7}{2}$ $J = 4$
46.256 (0.001)	46.22	—	57 {13}	78	—	7.00 (0.04) [0.07]	6.969	—	¹⁷⁷ $I = \frac{7}{2}$ $J = 4$
48.861 (0.001)	48.76	—	57 (1) [5]	82	—	36 (0.3) [1]	33.14	—	¹⁷⁷ $I = \frac{7}{2}$ $J = 3$
49.627 (0.001)	49.56	—	57 {13}	65	—	5.92 (0.04) [0.08]	5.244	—	¹⁷⁷ $I = \frac{7}{2}$ $J = 4$
54.815 (0.001)	54.71	—	57 {13}	69	—	20.6 (0.1) [0.2]	15.11	—	¹⁷⁷ $I = \frac{7}{2}$ $J = 4$
56.402 (0.001)	56.29	—	57 {13}	70	—	14.2 (0.08) [0.1]	14.06	—	¹⁷⁷ $I = \frac{7}{2}$ $J = 3$
57.082 (0.002)	57	—	57 {13}	65	—	4.23 (0.04) [0.02]	4.089	—	¹⁷⁷ $I = \frac{7}{2}$ $J = 4$
59.323 (0.002)	59.21	—	57 {13}	65	—	4.2535 (0.04) [0.03]	4.217143	—	¹⁷⁷ $I = \frac{7}{2}$ $J = 3$
62.228 (0.004)	62.15	—	57 {13}	65	—	1.63 (0.03) [0.02]	1.509	—	¹⁷⁷ $I = \frac{7}{2}$ $J = 3$
63.552 (0.001)	63.42	—	54.3 (0.4) [0.7]	55	—	70.2 (0.3) [0.7]	64.89	—	¹⁷⁷ $I = \frac{7}{2}$ $J = 4$
66.773 (0.007)	66.69	—	119 ^b (2)	65	—	41.6 ^b (0.5)	49.14	—	¹⁷⁷ $I = \frac{7}{2}$ $J = 3$
70.098 (0.009)	69.96	—	57 {13}	65	—	0.68 (0.03) [0.006]	0.471	—	¹⁷⁷ $I = \frac{7}{2}$ $J = 4$
71.440 (0.001)	71.29	—	57 {13}	54	—	14.08 (0.09) [0.1]	14.58	—	¹⁷⁷ $I = \frac{7}{2}$ $J = 4$
72.05 (0.02)	72.22	—	72 ^b (7)	65	—	2.2011 ^b (0.03)	1.669	—	¹⁷⁷ $I = \frac{7}{2}$ $J = 3$
75.672 (0.007)	75.41	—	57 {13}	65	—	2.9 (0.09) [0.2]	2.057	—	¹⁷⁷ $I = \frac{7}{2}$ $J = 3$

(Continued)

TABLE V (Continued)

Energy (eV)			Γ_γ (meV)			Γ_n (meV)			Isotope and Spin
RPI	ENDF/B-VI	Moxon et al. ²	RPI	ENDF/B-VI	Moxon et al. ²	RPI	ENDF/B-VI	Moxon et al. ²	
¹⁷⁷ Hf (Continued)									
76.135 (0.002)	75.99	—	57 {13}	65	—	15.0 (0.1) [0.3]	16.53	—	177 $I = \frac{7}{2}$ J = 4
82.35 (0.01)	82.33	—	57 {13}	65	—	0.64 (0.02) [0.02]	0.542	—	177 $I = \frac{7}{2}$ J = 4
84.762 (0.002)	84.56	—	57 {13}	75	—	23.5 (0.2) [0.3]	24.36	—	177 $I = \frac{7}{2}$ J = 4
85.31 (0.08)	85.25	—	57 {13}	65	—	0.38 (0.05) [0.07]	3.429	—	177 $I = \frac{7}{2}$ J = 3
86.861 (0.007)	86.73	—	57 {13}	65	—	1.14 (0.03) [0.02]	0.924	—	177 $I = \frac{7}{2}$ J = 4
88.639 (0.003)	88.51	—	57 {13}	65	—	4.58 (0.06) [0.04]	4.571	—	177 $I = \frac{7}{2}$ J = 3
93.312 (0.006)	93.13	—	57 {13}	65	—	4.7 (0.1) [0.1]	4.8	—	177 $I = \frac{7}{2}$ J = 3
97.208 (0.002)	97.01	—	98 (3) [13]	60	—	17.4 (0.1) [0.3]	19.2	—	177 $I = \frac{7}{2}$ J = 4
102.5 (0.1)	98.9	—	57 {13}	65	—	0.019 (0.002) [0.0003]	0.871	—	177 $I = \frac{7}{2}$ J = 4
103.258 (0.002)	103.07	—	57 {13}	63	—	59 (0.6) [1]	55.77	—	177 $I = \frac{7}{2}$ J = 3
111.56 (0.01)	111.5	—	57 {13}	65	—	2.3 (0.1) [0.02]	2.514	—	177 $I = \frac{7}{2}$ J = 3
112.030 (0.007)	111.96	—	57 {13}	65	—	4.1 (0.1) [0.04]	4	—	177 $I = \frac{7}{2}$ J = 4
115.243 (0.005)	115	—	57 {13}	65	—	4.05 (0.06) [0.06]	0.231	—	177 $I = \frac{7}{2}$ J = 4
121.34 (0.01)	121.2	—	57 {13}	65	—	4.2 (0.2) [0.06]	4.914	—	177 $I = \frac{7}{2}$ J = 3
122.1 (0.1)	122.7	—	57 {13}	65	—	2.5 (0.2) [0.1]	5.029	—	177 $I = \frac{7}{2}$ J = 3
122.18 (0.02)	122.8	—	57 {13}	65	—	0.54 (0.05) [0.009]	0.709	—	177 $I = \frac{7}{2}$ J = 3
123.88 (0.01)	123.7	—	57 {13}	65	—	8 (0.4) [1]	10.29	—	177 $I = \frac{7}{2}$ J = 3
126.36 (0.02)	126.2	—	57 {13}	65	—	0.82 (0.03) [0.02]	0.613	—	177 $I = \frac{7}{2}$ J = 4

(Continued)

TABLE V (Continued)

Energy (eV)			Γ_γ (meV)			Γ_n (meV)			Isotope and Spin
RPI	ENDF/B-VI	Moxon et al. ²	RPI	ENDF/B-VI	Moxon et al. ²	RPI	ENDF/B-VI	Moxon et al. ²	
¹⁷⁷ Hf (Continued)									
131.843 (0.002)	131.6	—	67 (1) [2]	66	—	59 (0.6) [2]	60.94	—	¹⁷⁷ $I = \frac{7}{2}$ $J = 3$
134.245 (0.006)	134	—	57 {13}	65	—	4.21 (0.08) [0.06]	3.733	—	¹⁷⁷ $I = \frac{7}{2}$ $J = 4$
136.27 (0.02)	136.2	—	57 {13}	65	—	1.7 (0.07) [0.2]	0.743	—	¹⁷⁷ $I = \frac{7}{2}$ $J = 3$
138.061 (0.005)	137.4	—	57 {13}	65	—	16.2 (0.3) [0.6]	12	—	¹⁷⁷ $I = \frac{7}{2}$ $J = 4$
141.351 (0.003)	141.1	—	57 {13}	54	—	21.1 (0.2) [0.2]	23.47	—	¹⁷⁷ $I = \frac{7}{2}$ $J = 4$
143.16 (0.02)	143.2	—	57 {13}	65	—	3.7 (0.2) [0.2]	4.96	—	¹⁷⁷ $I = \frac{7}{2}$ $J = 3$
143.84 (0.01)	143.7	—	57 {13}	65	—	9.5 (0.4) [0.6]	10.49	—	¹⁷⁷ $I = \frac{7}{2}$ $J = 4$
145.793 (0.006)	145.5	—	57 {13}	65	—	7.6 (0.1) [0.01]	7.371	—	¹⁷⁷ $I = \frac{7}{2}$ $J = 3$
148.765 (0.004)	148.5	—	57 {13}	65	—	21.0 (0.3) [0.5]	21.26	—	¹⁷⁷ $I = \frac{7}{2}$ $J = 3$
151.30 (0.03)	151.2	—	57 {13}	65	—	0.67 (0.05) [0.006]	0.409	—	¹⁷⁷ $I = \frac{7}{2}$ $J = 4$
152.67 (0.01)	152.9	—	57 {13}	65	—	3.82 (0.09) [0.08]	1.867	—	¹⁷⁷ $I = \frac{7}{2}$ $J = 4$
154.88 (0.02)	156.1	—	57 {13}	65	—	1.53 (0.07) [0.06]	3.2	—	¹⁷⁷ $I = \frac{7}{2}$ $J = 3$
160.229 (0.008)	160	—	57 {13}	65	—	3.91 (0.08) [0.05]	3.467	—	¹⁷⁷ $I = \frac{7}{2}$ $J = 4$
163.284 (0.003)	163	—	57 {13}	60	—	45.8 (0.6) [0.6]	44.57	—	¹⁷⁷ $I = \frac{7}{2}$ $J = 3$
167.596 (0.007)	167.3	—	57 {13}	65	—	9.346 (0.2) [0.1]	8.286	—	¹⁷⁷ $I = \frac{7}{2}$ $J = 3$
171.06 (0.01)	171	—	57 {13}	65	—	10 (0.2) [1]	12.91	—	¹⁷⁷ $I = \frac{7}{2}$ $J = 3$
174.326 (0.007)	174.2	—	57 {13}	65	—	27 (0.9) [3]	12.44	—	¹⁷⁷ $I = \frac{7}{2}$ $J = 4$
176.325 (0.008)	176.1	—	57 {13}	65	—	45 (1) [6]	56	—	¹⁷⁷ $I = \frac{7}{2}$ $J = 3$

(Continued)

TABLE V (Continued)

Energy (eV)			Γ_γ (meV)			Γ_n (meV)			Isotope and Spin
RPI	ENDF/B-VI	Moxon et al. ²	RPI	ENDF/B-VI	Moxon et al. ²	RPI	ENDF/B-VI	Moxon et al. ²	
¹⁷⁷ Hf (Continued)									
176.88 (0.03)	176.7	—	57 {13}	65	—	9 (1) [0.2]	44.44	—	177 $I = \frac{7}{2}$ J = 4
179.31 (0.06)	178.9	—	57 {13}	65	—	0.46 (0.04) [0.008]	0.667	—	177 $I = \frac{7}{2}$ J = 4
181.35 (0.01)	181.1	—	57 {13}	65	—	5.6 (0.1) [0.07]	5.156	—	177 $I = \frac{7}{2}$ J = 4
184.90 (0.02)	184.5	—	57 {13}	65	—	1.66 (0.07) [0.04]	1.262	—	177 $I = \frac{7}{2}$ J = 4
188.48 (.03)	188	—	57 {13}	65	—	1.8 (0.2) [0.02]	0.587	—	177 $I = \frac{7}{2}$ J = 4
193.012 (0.006)	192.7	—	57 {13}	65	—	15.0 (0.3) [0.07]	6.933	—	177 $I = \frac{7}{2}$ J = 4
194.400 (0.009)	194	—	57 {13}	65	—	9.8 (0.2) [0.1]	8.571	—	177 $I = \frac{7}{2}$ J = 3
199.488 (0.006)	199.1	—	57 {13}	72	—	21.0 (0.4) [0.2]	21.16	—	177 $I = \frac{7}{2}$ J = 4
¹⁷⁸ Hf									
-54.5	-54.5	—	60	60	—	1265.0	863.74	—	178 $I = 0$ J = $\frac{1}{2}$
7.7865 (0.0001)	7.78	7.7718 0.0017	53.0 (0.2) [0.1]	60	57.67 1.6	53.83 (0.08) [0.007]	50	52.13 1.42	178 $I = 0$ J = $\frac{1}{2}$
—	—	28.672 0.01	—	—	—	—	—	—	178 $I = 0$ J = $\frac{1}{2}$
104.904 (0.002)	104.8	—	53 ^c	51	—	7.16 (0.05) [0.08]	8.9	—	178 $I = 0$ J = $\frac{1}{2}$
164.707 (0.003)	164.6	—	53 ^c	51	—	13.5 (0.1) [0.06]	15	—	178 $I = 0$ J = $\frac{1}{2}$
¹⁷⁹ Hf									
-61.0	-61.0	—	55.9	55.9	—	23.46	23.46	—	179 $I = \frac{9}{2}$ J = 5
5.6885 (0.0002)	5.68	5.686 0.001	47 (0.4) [2]	62	62.64 2.96	4.27 (0.02) [0.04]	4.6	4.64 0.092	179 $I = \frac{9}{2}$ J = 5
17.6533 (0.0006)	17.65	17.658 0.0005	52 {8}	66	64.13 3.22	2.09 (0.01) [0.009]	2.333	2.065 0.031	179 $I = \frac{9}{2}$ J = 4

(Continued)

TABLE V (Continued)

Energy (eV)			Γ_γ (meV)			Γ_n (meV)			Isotope and Spin
RPI	ENDF/B-VI	Moxon et al. ²	RPI	ENDF/B-VI	Moxon et al. ²	RPI	ENDF/B-VI	Moxon et al. ²	
¹⁷⁹ Hf (Continued)									
19.131 (0.004)	19.13	19.1355 [0.0006]	52 {8}	66	—	0.124 (0.004) [0.0004]	0.109	0.107 [0.01]	179 $I = \frac{9}{2}$ J = 5
23.6577 (0.0006)	23.7	23.666 [0.008]	52 {8}	66	64.1 [9]	7.47 (0.05) [0.09]	7.546	7.68 [0.73]	179 $I = \frac{9}{2}$ J = 5
26.540 (0.002)	26.5	26.535 [0.011]	52 {8}	66	89.3 [10]	1.27 (0.01) [0.005]	1.333	1.14 [0.1]	179 $I = \frac{9}{2}$ J = 4
27.418 (0.004)	27.35	27.405 [0.012]	52 {8}	66	63.7 [11]	0.433 (0.009) [0.005]	0.391	0.415 [0.05]	179 $I = \frac{9}{2}$ J = 5
31.156 (0.006)	31.14	—	52 {8}	66	—	8.1447 (0.04) [0.06]	8.333	—	179 $I = \frac{9}{2}$ J = 4
36.520 (0.007)	36.5	—	52 {8}	66	—	26.00 (0.02) [0.04]	27.27	—	179 $I = \frac{9}{2}$ J = 5
40.1350 (0.0005)	40.12	—	61 (0.8) [3]	66	—	23.5 (0.1) [0.4]	22.73	—	179 $I = \frac{9}{2}$ J = 5
42.3270 (0.0007)	42.29	—	52 {8}	66	—	15.3 (0.08) [0.2]	14.44	—	179 $I = \frac{9}{2}$ J = 4
50.785 (0.005)	50.77	—	52 {8}	66	—	1.11 (0.03) [0.007]	1.455	—	179 $I = \frac{9}{2}$ J = 5
51.149 (0.009)	54.79	—	52 {8}	66	—	0.71 (0.03) [0.005]	5.889	—	179 $I = \frac{9}{2}$ J = 4
54.08 (0.01)	—	—	52 {8}	—	—	0.33 (0.02) [0.03]	—	—	179 $I = \frac{9}{2}$ J = 4
69.089 (0.002)	69.03	—	52 {8}	66	—	10.6 (0.09) [0.1]	11.11	—	179 $I = \frac{9}{2}$ J = 4
73.589 (0.002)	73.53	—	52 {8}	66	—	9.2 (0.1) [0.4]	8.889	—	179 $I = \frac{9}{2}$ J = 4
76.702 (0.005)	76.63	—	52 {8}	66	—	3.26 (0.06) [0.04]	2.818	—	179 $I = \frac{9}{2}$ J = 5
83.013 (0.004)	82.94	—	52 {8}	66	—	4.69 (0.07) [0.06]	6.667	—	179 $I = \frac{9}{2}$ J = 4
85.433 (0.003)	85.42	—	52 {8}	66	—	11.8 (0.2) [0.4]	6.364	—	179 $I = \frac{9}{2}$ J = 5
92.125 (0.004)	92.07	—	52 {8}	66	—	11.7 (0.2) [0.2]	55.56	—	179 $I = \frac{9}{2}$ J = 4
92.7852 (0.003)	—	—	52 {8}	—	—	27 (0.3) [0.6]	—	—	179 $I = \frac{9}{2}$ J = 5

(Continued)

TABLE V (Continued)

Energy (eV)			Γ_γ (meV)			Γ_n (meV)			Isotope and Spin
RPI	ENDF/B-VI	Moxon et al. ²	RPI	ENDF/B-VI	Moxon et al. ²	RPI	ENDF/B-VI	Moxon et al. ²	
¹⁷⁹ Hf (Continued)									
101.382 (0.001)	101.2	—	52 {8}	66	—	113.8 (0.7) [1]	118.2	—	179 I = $\frac{9}{2}$ J = 5
103.821 (0.006)	103.7	—	52 {8}	66	—	9.8 (0.2) [0.2]	9.091	—	179 I = $\frac{9}{2}$ J = 5
107.858 (0.004)	107.8	—	52 {8}	66	—	9.5 (0.1) [0.1]	14.44	—	179 I = $\frac{9}{2}$ J = 4
117.278 (0.002)	117.2	—	44 (1) [2]	66	—	31 (0.4) [1]	35.46	—	179 I = $\frac{9}{2}$ J = 5
120.165 (0.008)	120.1	—	52 {8}	66	—	3.46 (0.08) [0.03]	2.444	—	179 I = $\frac{9}{2}$ J = 4
121.86 (0.03)	121.9	—	52 {8}	66	—	3.7 (0.3) [0.07]	32.22	—	179 I = $\frac{9}{2}$ J = 4
122.689 (0.005)	122.6	—	52 {8}	66	—	15.8 (0.4) [0.4]	23.64	—	179 I = $\frac{9}{2}$ J = 5
130.024 (0.005)	129.9	—	52 {8}	66	—	10.2 (0.2) [0.09]	11.11	—	179 I = $\frac{9}{2}$ J = 4
137.426 (0.004)	137.2	—	52 {8}	66	—	36.6 (0.7) [0.7]	45.46	—	179 I = $\frac{9}{2}$ J = 5
144.341 (0.006)	144.2	—	52 {8}	66	—	32 (0.9) [2]	25.46	—	179 I = $\frac{9}{2}$ J = 5
147.103 (0.006)	147	—	52 {8}	66	—	12.2 (0.3) [0.05]	12.22	—	179 I = $\frac{9}{2}$ J = 4
156.393 (0.003)	156.3	—	58 (2) [2]	66	—	45 (0.7) [1]	40	—	179 I = $\frac{9}{2}$ J = 5
158.835 (0.008)	—	—	52 {8}	—	—	4.7 (0.1) [0.009]	—	—	179 I = $\frac{9}{2}$ J = 4
165.807 (0.005)	165.7	—	52 {8}	66	—	23.7 (0.4) [0.6]	20	—	179 I = $\frac{9}{2}$ J = 5
174.904 (0.008)	174.9	—	52 {8}	66	—	77 (2) [9]	144.4	—	179 I = $\frac{9}{2}$ J = 4
177.996 (0.006)	177.9	—	52 {8}	66	—	66 (2) [6]	25.46	—	179 I = $\frac{9}{2}$ J = 5
182.790 (0.005)	182.6	—	52 {8}	66	—	32.8 (0.6) [0.5]	53.33	—	179 I = $\frac{9}{2}$ J = 4
188.75 (0.02)	—	—	52 {8}	—	—	6.1 (0.4) [0.4]	—	—	179 I = $\frac{9}{2}$ J = 4

(Continued)

TABLE V (Continued)

Energy (eV)			Γ_γ (meV)			Γ_n (meV)			Isotope and Spin
RPI	ENDF/B-VI	Moxon et al. ²	RPI	ENDF/B-VI	Moxon et al. ²	RPI	ENDF/B-VI	Moxon et al. ²	
¹⁷⁹ Hf (Continued)									
189.953 (0.007)	188.5	—	52 {8}	66	—	20.2 (0.4) [0.5]	29.09	—	¹⁷⁹ I = $\frac{9}{2}$ J = 5
191.25 (0.06)	192.9	—	52 {8}	66	—	0.91 (0.08) [0.05]	5.556	—	¹⁷⁹ I = $\frac{9}{2}$ J = 4
198.052 (0.008)	197.9	—	52 {8}	66	—	16.1 (0.3) [0.2]	18.18	—	¹⁷⁹ I = $\frac{9}{2}$ J = 5
¹⁸⁰ Hf									
72.4640 (0.0007)	72.6	—	28.9 ^b (0.2)	46	—	63.3 ^b (0.2)	54	—	¹⁸⁰ I = 0 J = $\frac{1}{2}$
172.062 (0.003)	171.7	—	52 (0.4) [2]	78	—	115 (0.8) [2]	116	—	¹⁸⁰ I = 0 J = $\frac{1}{2}$

*RPI errors calculated from SAMMY are in (), errors propagated from resolution function uncertainties are in [], and the standard deviation is shown in { } where the average Γ_γ was used, errors from Moxon et al.² are in | |.

^aThese resonances in ¹⁷⁴Hf were fixed to the ENDF/B-VI values because of their very low cross-section values and overlapping neighboring resonances, which precluded them from analysis in this work.

^bThese resonances were fitted using a narrow energy range and manually changing values. They were then not allowed to vary during the fit over the full energy range as the values would run away due to the number of overlapping resonances. Therefore, the error due to resolution function uncertainties was not able to be determined.

^cOnly one resonance in ¹⁷⁸Hf was found to be sensitive to Γ_γ ; therefore, this value was applied to the other two resonances.

doublet was an indication of a lower detection efficiency for ¹⁷⁶Hf and ¹⁷⁸Hf neutron capture gamma rays relative to those from neutron capture in ¹⁷⁷Hf, which was used for flux normalization (at the 1.1-eV resonance).

The multiplicity distribution for these isotopes was examined to look for significant differences in average multiplicity. Differences in average multiplicity could indicate differences in detection efficiency, due to differences in the number of gamma rays emitted or in the energy of the gamma rays. Figure 3 shows a plot of the fraction of total counts versus multiplicity number. The counts for each unit of multiplicity were summed over a resonance for each of the isotopes ¹⁷⁶Hf, ¹⁷⁷Hf, and ¹⁷⁸Hf. The 8-eV resonance in the ¹⁷⁸Hf-enriched liquid sample data was used to obtain the multiplicity distribution for ¹⁷⁸Hf, and the 48-eV resonance in the ¹⁷⁶Hf-enriched liquid sample data was used for ¹⁷⁶Hf. The 1-eV resonance was used to get the ¹⁷⁷Hf multiplicity distribution. This plot shows that ¹⁷⁷Hf has a higher average multiplicity (4.2) than ¹⁷⁶Hf and ¹⁷⁸Hf (3.8). This means that on average a neutron capture in ¹⁷⁷Hf produces ~11% more gamma rays than in ¹⁷⁶Hf or ¹⁷⁸Hf. This higher number of capture gamma rays should increase the chance for detecting a capture event in ¹⁷⁷Hf

relative to ¹⁷⁶Hf or ¹⁷⁸Hf. The binding energy for each isotope can also have an effect on detection efficiency by determining the total energy emitted by the capture gamma rays. Table VI shows the binding energy for ¹⁷⁶Hf, ¹⁷⁷Hf, and ¹⁷⁸Hf along with the average multiplicity at selected resonances near 8 eV. The higher binding energy of ¹⁷⁷Hf, along with the higher average multiplicity, are expected to increase the probability of detection due to more energy and gamma rays being released on average for each capture event. This effect would cause the detection efficiency for ¹⁷⁷Hf to be relatively larger, and thus, a lower yield would be observed for ¹⁷⁶Hf and ¹⁷⁸Hf resonances relative to ¹⁷⁷Hf resonances. This trend is also in agreement with detection efficiency calculations based on capture gamma-ray cascades in hafnium done using the DICEBOX code.^{11,12}

SAMMY was used to fit a normalization factor that would correct for the difference in detection efficiency. This was accomplished by using the resonance parameters fitted to the liquid transmission data as input to SAMMY. A combined fit of all capture data sets was then run allowing only normalization to vary. This analysis determined there was a 24% difference between the yield data and the SAMMY calculated yield from the

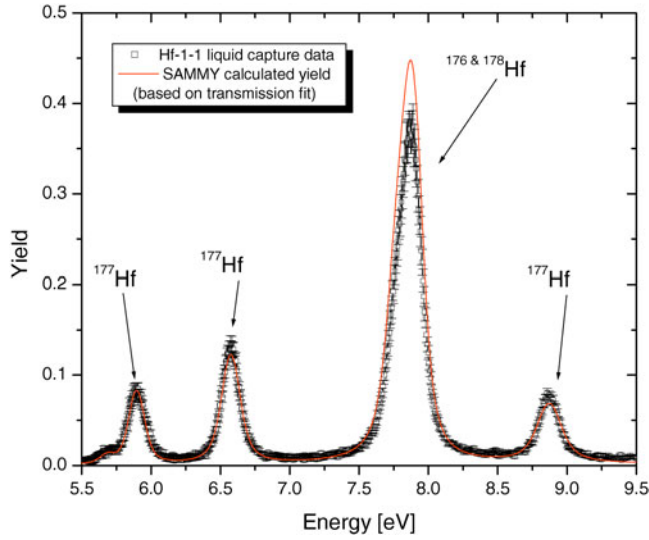


Fig. 2. ¹⁷⁶Hf-enriched liquid capture data compared to calculated yield based on 8-eV resonance parameters fitted to transmission data showing the normalization problem.

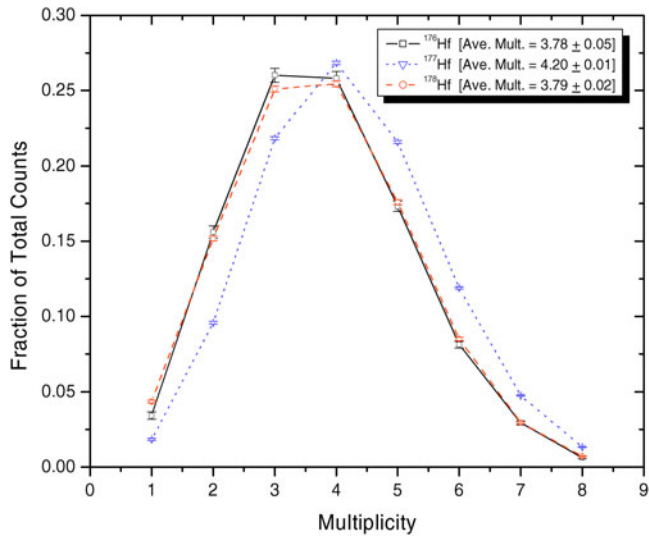


Fig. 3. Multiplicity distribution for ¹⁷⁶Hf, ¹⁷⁷Hf, and ¹⁷⁸Hf.

transmission fitted parameters. The ¹⁷⁶Hf and ¹⁷⁸Hf detection efficiencies were comparable because of their similar average multiplicities and binding energies. This normalization factor was then used to correct the yield data.

A combined transmission and capture data analysis was then performed using the corrected capture data. This analysis included both first- and second-generation liquid sample data from capture and transmission experiments. Figure 4 shows a plot of ¹⁷⁶Hf-enriched liquid sample capture data with calculated curves based on both

TABLE VI
Binding Energy and Average Multiplicity for ¹⁷⁶Hf, ¹⁷⁷Hf, and ¹⁷⁸Hf*

Isotope	Binding Energy (MeV)	Average Multiplicity
¹⁷⁶ Hf	6.3833 ± 0.002	3.78 ± 0.05
¹⁷⁷ Hf	7.6263 ± 0.0009	4.20 ± 0.01
¹⁷⁸ Hf	6.0998 ± 0.0008	3.79 ± 0.02

*From Ref. 15.

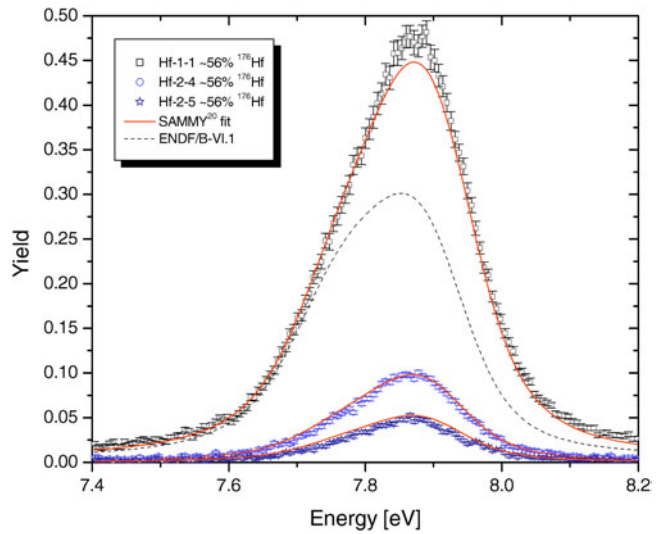


Fig. 4. ¹⁷⁶Hf-enriched liquid capture samples with SAMMY calculated yield from fitted resonance parameters and calculated yield based on ENDF/B-VI.1 parameters.

ENDF/B-VI.1 resonance parameters and those determined from this analysis. The fit to the ¹⁷⁶Hf-enriched samples is not as good as that to the ¹⁷⁸Hf-enriched samples. Figure 4 shows the fit slightly underpredicting the yield of the thickest sample (Hf-1-1) and overpredicting the two thinner samples (Hf-2-4 and Hf-2-5). These inconsistencies may be due to inaccuracies in the solution contents of the ¹⁷⁶Hf-enriched liquid samples. The fits for these samples are still acceptable and are a significant improvement over the yields calculated from the ENDF/B-VI.1 values, as shown in Fig. 4. Figure 5 shows the transmission results for the ¹⁷⁶Hf-enriched samples, which show good agreement between experiment and calculated values. Figure 6 shows the capture results for ¹⁷⁸Hf-enriched samples compared to ENDF/B-VI.1 values. Figure 6 also shows significantly better agreement between experiment and calculated yields for the ¹⁷⁸Hf parameters derived in this analysis as compared to those based on ENDF/B-VI.1 parameters. Figure 7 shows the

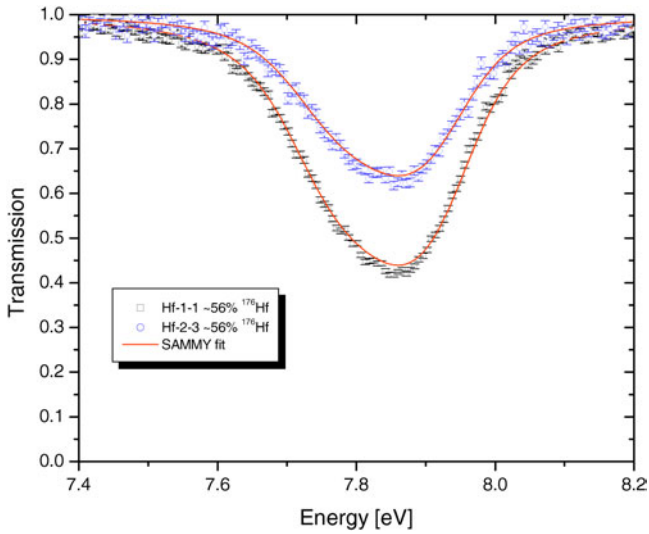


Fig. 5. ^{176}Hf -enriched liquid transmission samples with SAMMY calculated transmission from fitted resonance parameters.

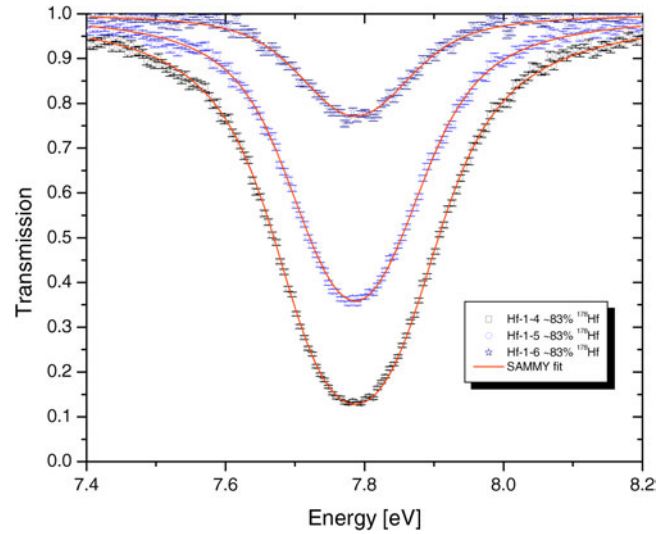


Fig. 7. ^{178}Hf -enriched liquid transmission samples with SAMMY calculated transmission from fitted resonance parameters.

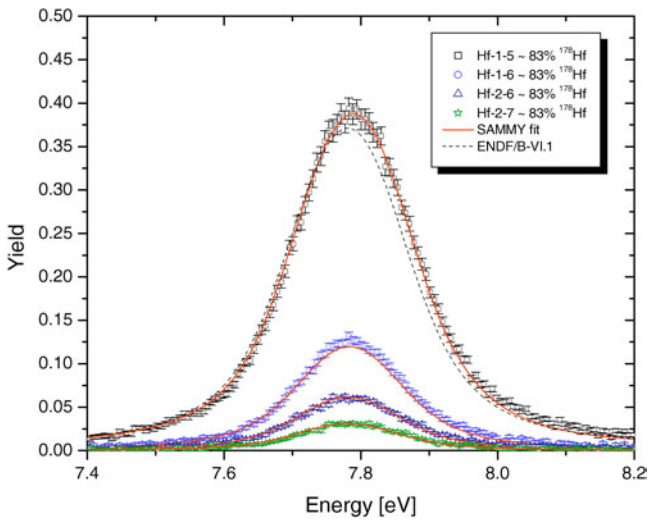


Fig. 6. ^{178}Hf -enriched liquid capture samples with SAMMY calculated yield from fitted resonance parameters and calculated yield based on ENDF/B-VI.1 parameters.

transmission results for the ^{178}Hf -enriched samples, which also show good agreement between experiment and calculated transmission values, based on resonance parameters determined in this analysis.

V. RESULTS

Resonance parameters determined from the previously described analyses are presented in Table V, shown

as the RPI resonance parameters. Two error values are reported for the RPI resonance parameters. The error value determined by SAMMY is shown in parentheses and is based primarily on the statistical accuracy of the experimental data used in the fit. The error value shown in square brackets is an estimate of the error in the resonance parameters due to uncertainties in the resolution function. Reference 3 contains a detailed description of the methods used to calculate the uncertainties shown in Table V.

Table V also shows the ENDF/B-VI parameters, which were used as starting values for the SAMMY analysis, and the parameters reported from Moxon et al.² The Γ_γ values with errors in curly brackets { } are those resonances that were deemed insensitive to changes in Γ_γ and were set to the average Γ_γ value for that isotope. The error quoted for these average values of Γ_γ is 1σ .

The resonance parameters determined for the ^{176}Hf and ^{178}Hf resonances near 8 eV are significantly different from the few previous measurements available. The biggest change is in the Γ_n value in the ^{176}Hf resonance at 7.8891 eV. The value quoted by Moxon et al. of 4.71 meV is approximately one-third the value determined in this analysis of 10.15 meV. The value quoted by Moxon et al., which is also the ENDF/B-VI value, is quoted with an extremely high error ($>100\%$), and it is therefore not surprising to see a large change in this parameter. This analysis provides a Γ_n value with a significantly lower uncertainty than was previously available. As recommended by Moxon et al., this analysis has led to the same conclusion that a more highly enriched ^{176}Hf sample would allow for an even more accurate set of resonance parameters to be determined for this resonance.

TABLE VII
Hafnium Thermal Cross Section Based on ENDF/B-VI
and RPI Resonance Parameters

Thermal Cross Section (σ_T at 0.0253 eV)	
ENDF/B-VI	114.5 b
RPI	115.3 \pm 0.8 b

The thermal cross sections based on the fitted RPI parameters and the ENDF/B-VI parameters are shown in Table VII. As expected, the RPI value is within the quoted error of the ENDF/B-VI value. This is due to good agreement between the ENDF/B-VI and fitted RPI resonance parameters at low energies. The majority of previous hafnium measurements was done in the thermal energy region, making the lower-energy hafnium resonance parameters quite reliable, with the exception of the two resonances at 8 eV.

V.A. Resonance Integrals

Resonance integrals for each of the hafnium isotopes analyzed were calculated along with errors. The resonance integrals (shown in Table VIII) were calculated based on the resonance parameters determined in this analysis. ENDF/B-VI resonance parameters were used outside the energy range analyzed in this work for the resonance integral calculations. NJOY (Ref. 13) and INTER (Ref. 14) were used to calculate the resonance integral for the hafnium isotopes. Table VIII shows the calculated resonance integral for each of the hafnium isotopes analyzed compared to those based on other evaluated hafnium resonance parameters. As is shown in Table VIII, significant changes in some of the hafnium isotopic resonance integrals were calculated based on the resonance parameters determined in this analysis. The elemental hafnium resonance integral calculated from

the abundance weighted sum of the isotopic resonance integrals also differs from resonance integrals calculated from other data sets. Table IX shows the resonance integrals calculated from ENDF/B-VI and RPI resonance parameters with an integration region from 0.5 to 200 eV. This was calculated to show the energy region that includes only resonances that were analyzed in this work. The errors calculated are based on resonance errors listed in Table V.

VI. CONCLUSIONS

This paper presents the results of both capture and transmission experiments using various hafnium samples. These experiments provided energy-dependent transmission and yield data that were analyzed using the R-matrix Bayesian fitting code SAMMY. The transmission experiments were done utilizing a ^6Li glass scintillation detector at an $\sim 15\text{-m}$ flight path for low-energy measurements (0.005 to 10 eV) and a similar detector at $\sim 25\text{ m}$ for higher-energy measurements (10 to 200 eV). A 16-section NaI(Tl) multiplicity detector was used for the capture experiments at a flight path of $\sim 25\text{ m}$.

The samples used in these experiments were various thicknesses of metallic hafnium and deuterated nitric acid solutions of isotope-enriched hafnium. The isotope-enriched samples were designed to provide experimental data that could be used to determine resonance parameters for the overlapping resonances of ^{176}Hf and ^{178}Hf at $\sim 8\text{ eV}$. The liquid solution samples were needed to provide sufficiently thin samples to prevent saturation or blacking out of the 8-eV resonance pair in capture and transmission experiments. Enriched samples were used to determine the individual contribution of ^{176}Hf and ^{178}Hf to the resonance pair. The only previously found ^{176}Hf parameters for the 8-eV resonance were from measurements done by Moxon et al.,² which have an extremely high quoted error and are referred to as “not well known” in the report. This analysis provides a much more accurate set of resonance parameters for this 8-eV

TABLE VIII
Resonance Integrals Calculated from Resonance Parameters Determined in This Analysis (Labeled RPI)
Compared with Those from Other Evaluated Hafnium Resonance Parameters*

	Values (b)						
	^{174}Hf	^{176}Hf	^{177}Hf	^{178}Hf	^{179}Hf	^{180}Hf	Natural
JEF-2.2	320.3	612.8	7232	1922	543.1	35.44	1983
JENDL-3.2	361.8	892.7	7209	1914	521.6	33.85	1987
ENDF/B-VI	355.1	400.2	7221	1915	548.6	34.28	1968
RPI	375 \pm 20	692 \pm 2	7196 \pm 8	1872 \pm 4	506 \pm 3	28.8 \pm 0.1	1959 \pm 2

*All were integrated from 0.5×10^5 to 1.0×10^5 eV.

TABLE IX
Resonance Integrals Calculated from Resonance Parameters Determined in this Analysis (Labeled RPI)
and from ENDF/B-VI Parameters, Integrated from 0.5 to 200 eV

	Values (b)						
	^{174}Hf	^{176}Hf	^{177}Hf	^{178}Hf	^{179}Hf	^{180}Hf	Natural
ENDF/B-VI	324.5	381.6	7158	1902	506.7	30.66	1944.8
RPI	345 ± 20	673 ± 2	7139 ± 8	1859 ± 4	464 ± 3	25.2 ± 0.1	1937 ± 2

doublet. A combined analysis of capture and transmission data using SAMMY was performed to determine resonance parameters for all stable isotopes of hafnium in the energy range of 0.005 to 200 eV.

Resonance integrals for each hafnium isotope, based on the fitted resonance parameters, were calculated using the NJOY and INTER codes. A method to estimate the error on the resonance integral due to the error on resonance parameters is also presented. The ^{176}Hf resonance integral, based on this work, is $\sim 73\%$ higher than that using ENDF/B-VI parameters. This change is primarily due to the significant change in ^{176}Hf resonance parameters near 8 eV. This change is not surprising, given the small amount of experimental data available for this pair of resonances and the high level of uncertainty in previous work. A much smaller change in the ^{178}Hf resonance integral, which is $\sim 2\%$ lower than ENDF/B-VI, is also primarily due to the changes in the ^{178}Hf resonance parameters near 8 eV.

The hafnium experimental data and resonance parameters provided are a significant improvement over previous measurements, due to improved sample design, experimental resolution, and analysis tools.

REFERENCES

1. H. I. LIOU, J. RAINWATER, G. HACKEN, and U. N. SINGH, *Phys. Rev. C*, **11**, 2022 (1975).
2. M. C. MOXON, D. A. J. ENDACOTT, T. J. HASTE, J. E. JOLLY, J. E. LYNN, and M. G. SOWERBY, "Differential Neutron Cross-Sections of Natural Hafnium and Its Isotopes for Neutron Energies Up to 30 eV," AERE-R 7684, United Kingdom Atomic Energy Authority (1974).
3. M. TRBOVICH, "Hafnium Cross Sections and Resonance Analysis," PhD Thesis, Rensselaer Polytechnic Institute (2003).
4. R. C. BLOCK, Y. DANON, R. E. SLOVACEK, C. J. WERNER, G. YOUK, J. A. BURKE, N. J. DRINDAK, F. FEINER, J. A. HELM, J. C. SAYRES, and K. W. SEEMAN, "Neutron Time-of-Flight Measurements at the Rensselaer LINAC," *Proc. Int. Conf. Nuclear Data for Science and Technology*, Gatlinburg, Tennessee, May 9–13, 1994, p. 81, American Nuclear Society (1994).
5. Y. DANON, "Design and Construction of the RPI Enhanced Thermal Neutron Target and Thermal Cross Section Measurements of Rare Earth Isotopes," PhD Thesis, Rensselaer Polytechnic Institute (1993).
6. B. E. MORETTI, "Molybdenum Neutron Transmission Measurements and the Development of an Enhanced Resolution Neutron Target," PhD Thesis, Rensselaer Polytechnic Institute (1996).
7. M. E. OVERBERG, "Development of an Improved Epithermal Neutron Target and Measurement of the Resolution Function to 350 eV," MS Thesis, Rensselaer Polytechnic Institute (1997).
8. N. J. DRINDAK, "A Multiplicity Detector for Neutron Capture Measurements," Masters Thesis, Rensselaer Polytechnic Institute (1987).
9. N. M. LARSON, "Updated Users Guide for SAMMY: Multilevel R-Matrix Fits to Neutron Data Using Bayes' Equations," ORNL/TM-9179/R5, Oak Ridge National Laboratory (2000).
10. D. P. BARRY, "Neodymium Neutron Transmission and Capture Measurements and the Design of an Improved Resolution Transmission Detector," PhD Thesis, Rensselaer Polytechnic Institute (2003).
11. M. LUBERT, Rensselaer Polytechnic Institute, Personal Communication.
12. F. BECVÁR, *Nucl. Instrum. Methods A*, **417**, 434 (1998); see also *Nucl. Instrum. Methods*, **105**, 113 (2000).
13. R. E. MacFARLANE and D. W. MUIR, "The NJOY Nuclear Data Processing System Version 91," LA-12740-M, Los Alamos National Laboratory (Oct. 1994).
14. C. L. DUNFORD, "ENDF Utility Codes Release 6.12," Informal report (Apr. 2001).
15. S. F. MUGHABGHAB, M. DIVADEENAM, and N. E. HOLDEN, *Neutron Cross Sections*, Academic Press, New York and London (1984).